Supporting Information

A New Broad-Band Infrared Window Material CdPbOCl$_2$ with Excellent Comprehensive Properties

Chen Bai,[a,b] Bingliang Cheng,[b,c] Kewang Zhang,[b] Min Zhang,[b,c] Shilie Pan*[b,c] and Junjie Li*[b,c]

[a]College of Chemistry and Chemical Engineering, Xinjiang Normal University, 102 Xinyi Road, Urumqi 830054, China.

[b]CAS Key Laboratory of Functional Materials and Devices for Special Environments, Xinjiang Key Laboratory of Electronic Information Materials and Devices.

Xinjiang Technical Institute of Physics and Chemistry CAS,40-1 South Beijing Road, Urumqi 830011, China.

[b]Center of Materials Science and Optoelectronics Engineering, University of Chinses Academy of Sciences, Beijing 100049, China.

E-mail: slpan@ms.xjb.ac.cn; lijunjie@ms.xjb.ac.cn

Contents

1. Experimental Section

1.1. Sample Fabrication

The raw reagents ($CdCl_2$, PbO, $PbCl_2$) with a purity of 99.0 % were purchased from Aladdin Industrial Corporation, and used without further purification. All the raw reagents are stored in a glove box with controlled moisture and oxygen levels below 0.1 ppm.

Fabrication of CPOC single crystals.

CPOC single crystals for single-crystal X-ray diffraction measurement were fabricated by high-temperature spontaneous crystallization method in vacuum-sealed silica tubes. The detailed synthesis process is as follows: (1) A mixture of $CdCl_2$ (0.259 g, 1.413 mmol), $PbCl_2$ (0.131 g, 0.417mmol), and PbO (0.105 g, 0.47mmol) was weighted, ground, and then loaded into a graphite crucible with an inner diameter of 7 mm; (2) The crucible was transferred into a quartz tube, and the quartz tube was sealed with a methane-oxygen flame under a high vacuum of 10^{-3} Pa. (3) The sealed tube was heated to 500 °C in 10 h in a computer-controlled furnace, and kept at this temperature for 48 h, and then cooled to room temperature at a rate of 1.0 °C / h. Finally, the colorless strip-shaped CPOC crystals were obtained. The millimeter-scale CPOC single crystals were grown by high temperature flux method. The mixture of $CdCl_2$ and PbO with a molar ratio of 2 : 1 was placed in a platinum crucible, which was rapidly heated to 580 °C and dwelled for 24 h for homogenization in a programmable temperature-controlled growth furnace. Then, the furnace was then cooled to 560 °C over 2 h, followed by cooling to 526 °C at a rate of 2 °C / h. At

560 °C, a crystalline CPOC seed was placed into the central portion of the melt surface to induce crystal growth. After 10 h growth, the crystal was lifted from the surface of solution and cooled to room temperature in 6 days.

Synthesis of Pure Phase CPOC Powder Samples.

Polycrystalline CPOC powder samples were synthesized by the solid-state reaction method by mixing $CdCl_2$ and PbO with a molar ratio of 1 : 1 in vacuum-sealed silica tubes. The mixture was heated to 500 °C in 10 h and dwelled for 20 h. After that, the temperature was gradually cooled to 300 °C at a rate of 3 °C / h, and then cooled to room temperature naturally.

1.2. Structure Characterizations

A Bruker SMART APEX II 4K CCD diffractometer with Mo Kα radiation (λ = 0.71073 Å) was used to collect the single-crystal X-ray Diffraction (XRD) data of CPOC at 296 (2) K, and the data were integrated with a SAINT program. The direct methods and SHELXTL system[1] were used to solve and refine the crystal structure, respectively. All of the positions of the atoms were refined by full-matrix least-squares techniques.[2, 3] The structure and purity of the pure phase CPOC powder samples were confirmed by powder X-ray diffraction (XRD), which was performed on a Bruker D2 PHASER diffractometer equipped with Cu Kα radiation at room temperature. The diffraction patterns were recorded with the 2θ range from 10 to 70 °. The scanning step width was 0.01 ° and the scanning rate was 1 s / step.

1.3. The Characterizations of Optical Properties

Raman Spectrum Measurements

The Raman spectrum was collected with CPOC single crystal on a LABRAM HR Evolution spectrometer equipped with a CCD detector using 532 nm radiations from a diode laser. The CPOC single crystal was loaded on a glass slide, and an objective lens was used to choose the measured area of the single crystal. A beam with a diameter of 35 μm and the maximum power of 60 mW were used. The data collection was finished in 15 s.

Transmittance Spectrum.

Transmission spectrum was measured on a 0.5 mm thick CPOC transparent crystal plate in the range 190-2500 nm (UV-Vis-NIR) by a SolidSpec-3700 UV spectrophotometer, and in the range 4000 to 400 cm^{-1} by a SHIMADZU IRAffinity-1 Fourier transform infrared spectrometer (MIR).

UV-vis-NIR Diffuse-reflectance Spectroscopy

The UV−vis−NIR diffuse reflectance spectrum for pure phase CPOC powder samples was characterized by a Shimadzu SolidSpec-3700 DUV spectrophotometer in an atmosphere of flowing nitrogen to determine the accurate absorption edge of CPOC at room temperature. Tetrafluoroethylene was used as a diffuse reflectance standard. The reflectance spectrum was converted to absorbance using the Kubelka−Munk function,[4, 5] $F(R) = (1 - R)^2 / (2R)$, where R is the reflectance.[6-8]

Laser-Induced Damage Threshold

Laser-induced damage threshold (LIDT) of CPOC was evaluated using a 1064 nm Q-switch laser and the commercial AgGaS$_2$ was used as a reference. The powder samples were surrounded by a 1 mm thick silicone pad with an 8 mm diameter hole

and pressed between two glass slides. Then, they were fixed in a light-tight box with the plane surface explored under a pulsed laser beam (1064 nm, 10 ns). The pulse energy was raised from 0.2 mJ and stopped when obvious damage was discovered under a microscope after the irradiation.

1.4. The Characterizations of Physical and Chemical Properties

Vickers Hardness

The Vickers hardness of CPOC was tested using an FM-700 automatic micro-Vickers hardness tester with a nominal test force of 0.9807 N.

Air and Humidity Stability

The air and humidity stability of CPOC were evaluated in a KS-50 high and low temperature alternating temperature-humidity test chamber (Nanjing Kenfan Electronic Technology Co. Ltd.). To test the air stability, the XRD patterns of CPOC powder samples before and after air-exposure for six months were investigated. To evaluate the humidity stability, CPOC single crystals and powder samples were put into the high and low temperature alternating temperature-humidity test chamber at 30 ºC with a humidity of 50 % for 10 and 20 h, respectively. The corresponding XRD patterns and IR transmission spectra were characterized.

Thermal Behavior

The gravimetric analysis (TGA) and differential scanning calorimetry (DSC) were carried out on a NETZSCH STA 449F3 thermal analyzer instrument at a temperature range of 40−900 °C with a heating rate of 5 °C /min in an atmosphere of flowing N_2.

1.5. Theoretical Calculations

Using the plane-wave pseudopotential method implemented in the CASTEP, the electronic structure of CPOC was investigated on density functional theory (DFT).[9, 10] The exchange-correlation potential[11] was treated by the Perdew-Burke-Ernzerhof (PBE) method in the generalized gradient approximation (GGA) and the interactions between the ionic cores and electrons were described by norm-conserving pseudopotential (NCP).[12] The following orbital electrons were treated as valence electrons: Cd $4d^{10}\,5s^2$, Pb $6s^2\,6p^2$, and O $2s^2\,2p^4$, Cl $3s^2\,3p^5$. To achieve convergence of the calculation results, the plane-wave energy cutoff was set to 700 eV. Meanwhile, Monkhorst-Pack k-point meshes ($4 \times 4 \times 2$) with a density of fewer than 0.04 Å^{-1} in the Brillouin zone (BZ) were adopted. The other calculation parameters and convergent criteria were set by the default values of the CASTEP code. In addition, in order to demonstrate the stability of the $CdPbOCl_2$ structure and the wide infrared transmission, calculations of the phonon spectrum and the theoretical infrared of the title compound were performed.

2. Tables and Figures

Table S1. Crystallographic data and structure refinement for $CdPbOCl_2$.

Table S2. The final Atomic coordinates and equivalent isotropic displacement parameters for $CdPbOCl_2$. U_{eq} is defined as one-third of the trace of the orthogonalized U_{ij} tensor, and the Bond Valence Sum for each atom in asymmetric unit.

Table S3. Bond lengths [Å] and angles [deg] for $CdPbOCl_2$.

Figure S1. The Cd coordination forms in $C_3H_9Cd_{1.5}Cl_3O_4P$, $CdOHCl$, $Cd(IO_3)Cl$ and $Cd_5(BO_3)_3Cl$.

Figure S2. The Pb coordination forms in $Pb_3O_2Cl_2$, $Pb_{17}O_8Cl_{18}$ and $Ba_{27}Pb_8O_8Cl_{54}$.

Figure S3. The energy-dispersive X-ray spectroscopy of $CdPbOCl_2$.

Figure S4. Crystal structure of $CdPb_2O_2Cl_2$. (a-b) The coordination of Cd and Pb atoms; (c-d) The Structure of $CdPb_2O_2Cl_2$ viewed along the b-axis and c-axis.

Figure S5. UV-vis-NIR diffuse spectrum and experiment band gap of $CdPbOCl_2$.

Figure S6. XRD comparison of $CdPbOCl_2$ powder before and after being placed in air for six months.

Figure S7. (a) TG-DSC curves of $CdPbOCl_2$; (b) The powder XRD results before and after heating at ~560 °C.

Figure S8. (a) Weight loss of $CdPbOCl_2$ single crystals placed at 50% humidity for 5h, 10h, 15h and 20h; (b-d) Optical images of $CdPbOCl_2$ single crystal placed at 50% humidity for 10h (c) and 20h (d).

Figure S9. Calculated phonon spectrum of $CdPbOCl_2$

Table 1 Crystallographic data and structure refinement for $CdPbOCl_2$.

Empirical formula	$CdPbOCl_2$
Formula weight	406.5158
Space group	$P2_1/c$
$a/Å$	6.336 (3)
$b/Å$	11.981(6)
$c/Å$	5.927(3)
$\alpha=\gamma/°$	90°
$\beta/°$	95.675(7)°
$V/Å^3$	447.72(40)
Z	4
ρ_{calc} g/cm^3	6.030
μ/mm^{-1}	43.300
$F(000)$	688
Radiation	MoKα (λ = 0.71073)
2θ range for data collection/°	6.462 to 55.152
Index ranges	$-8 \leq h \leq 8, -15 \leq k \leq 12, -5 \leq l \leq 7$
Reflections collected	2717
Independent reflections	1028 [R_{int}= 0.0612, R_{sigma}= 0.0733]
Data/restraints/parameters	1028/0/47
GOF on F^2	1.002
Final R indexes [$I>=2\sigma (I)$][a]	$R_1 = 0.0434, wR_2 = 0.0991$
Final R indexes [all data]	$R_1 = 0.0541, wR_2 = 0.1056$

[a] $R_1 = \Sigma||F_o|-|F_c||/\Sigma|F_o|$ and $wR_2 = [\Sigma w(F_o^2 - F_c^2)^2/ \Sigma w\ F_o^4]^{1/2}$ for $F_o^2 > 2\sigma(F_o^2)$.

Table S2. The final atomic coordinates ($\times 10^4$) and equivalent isotropic displacement parameters ($\text{Å}^2 \times 10^3$) for CdPbOCl$_2$, the Bond Valence Sum for each atom in asymmetric unit.

Atom	x	y	z	U(eq)[a]	BVS[b]
Cd(1)	4679.7(17)	6514.5(8)	6324.4(16)	16.3(3)	1.69
Pb(1)	8322.2(9)	8566.8(4)	6807.7(8)	16.4(3)	2.14
O(1)	6538(15)	7547(7)	4133(14)	15(2)	2.20
Cl(1)	6250(6)	4605(3)	7651(6)	22.5(8)	0.72
Cl(2)	943(7)	6550(3)	7140(6)	24.1(8)	0.91

[a]Ueq is defined as one-third of the trace of the orthogonalized Uij tensor.

[b]Bond valence sums are calculated by using bond-valence theory (Si = exp[(Ro−Ri)/B], where Ro is an empirical constant, Ri is the length of bond I (in angstroms), and B = 0.37).

Table S3. Bond lengths [Å] and angles [°] for CdPbOCl$_2$.

Cd(1)-O(1)	2.208(9)	Cl(1)#2-Cd(1)-Pb(1)	121.63(9)
Cd(1)-O(1)#1	2.239(9)	Cl(1)-Cd(1)-Cl(1)#2	82.64(12)
Cd(1)-Cl(1)#2	2.726(4)	Cl(2)-Cd(1)-Pb(1)	129.32(9)
Cd(1)-Cl(1)	2.582(4)	Cl(2)-Cd(1)-Cl(1)#2	92.48(13)
Cd(1)-Cl(2)	2.475(5)	Cl(2)-Cd(1)-Cl(1)	107.48(12)
Pb(1)-O(1)#1	2.295(9)	O(1)-Pb(1)-Cd(1)	40.6(2)
Pb(1)-O(1)	2.220(8)	O(1)#1-Pb(1)-Cd(1)	41.6(2)
Pb(1)-Cl(2)#3	2.928(4)	O(1)-Pb(1)-O(1)#1	82.1(2)
		O(1)-Pb(1)-Cl(2)#3	80.7(2)
O(1)#1-Cd(1)-Pb(1)	42.9(2)	O(1)#1-Pb(1)-Cl(2)#3	77.8(2)
O(1)-Cd(1)-Pb(1)	40.8(2)	Cl(2)#3-Pb(1)-Cd(1)	77.28(9)
O(1)-Cd(1)-O(1)#1	83.7(2)	Cd(1)-O(1)-Cd(1)#4	116.9(4)
O(1)#1-Cd(1)-Cl(1)#2	160.7(3)	Cd(1)#4-O(1)-Pb(1)#4	95.5(3)
O(1)-Cd(1)-Cl(1)	117.9(3)	Cd(1)-O(1)-Pb(1)	98.6(3)
O(1)-Cd(1)-Cl(1)#2	81.4(2)	Cd(1)-O(1)-Pb(1)#4	110.4(4)
O(1)#1-Cd(1)-Cl(1)	93.7(2)	Pb(1)-O(1)-Cd(1)#4	116.4(4)
O(1)-Cd(1)-Cl(2)	132.8(3)	Pb(1)-O(1)-Pb(1)#4	120.2(4)
O(1)#1-Cd(1)-Cl(2)	106.6(3)	Cd(1)-Cl(1)-Cd(1)#2	97.36(12)
Cl(1)-Cd(1)-Pb(1)	112.72(10)	Cd(1)-Cl(2)-Pb(1)#5	123.42(14)

Symmetry transformations used to generate equivalent atoms:

[#1] x,-y+3/2,z+1/2   [#2] -x+1,-y+1,-z+1   [#3] x+1,y,z

[#4] x,-y+3/2,z-1/2   [#5] x-1,y,z
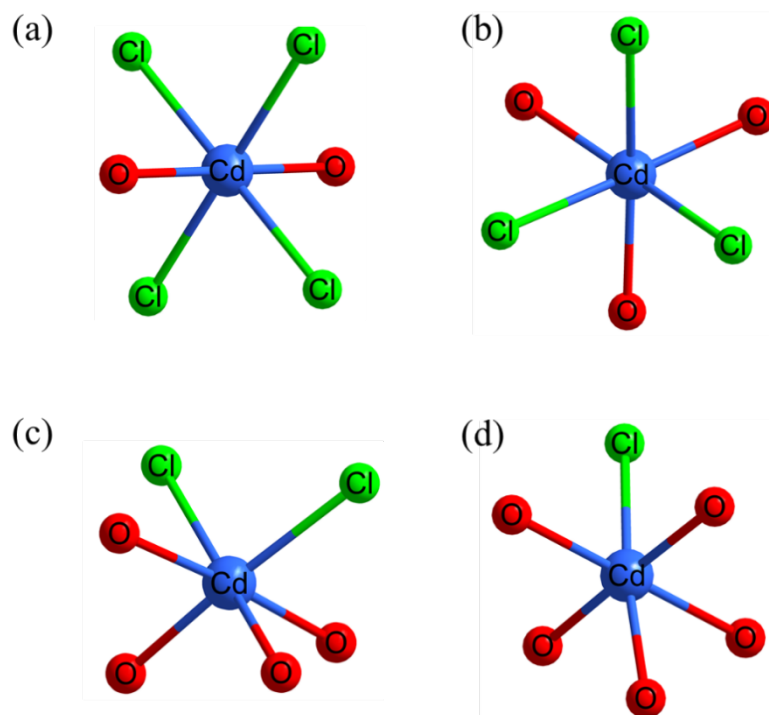
Figure S1. (a) The structure of $[CdO_2Cl_4]$ in $C_3H_9Cd_{1.5}Cl_3O_4P$;[13] (b) The structure of $[CdO_3Cl_3]$ in CdOHCl;[14] (c) The structure of $[CdO_4Cl_2]$ in $Cd(IO_3)Cl$;[15] (d) The structure of $[CdO_5Cl_1]$ in $Cd_5(BO_3)_3Cl$.[16]
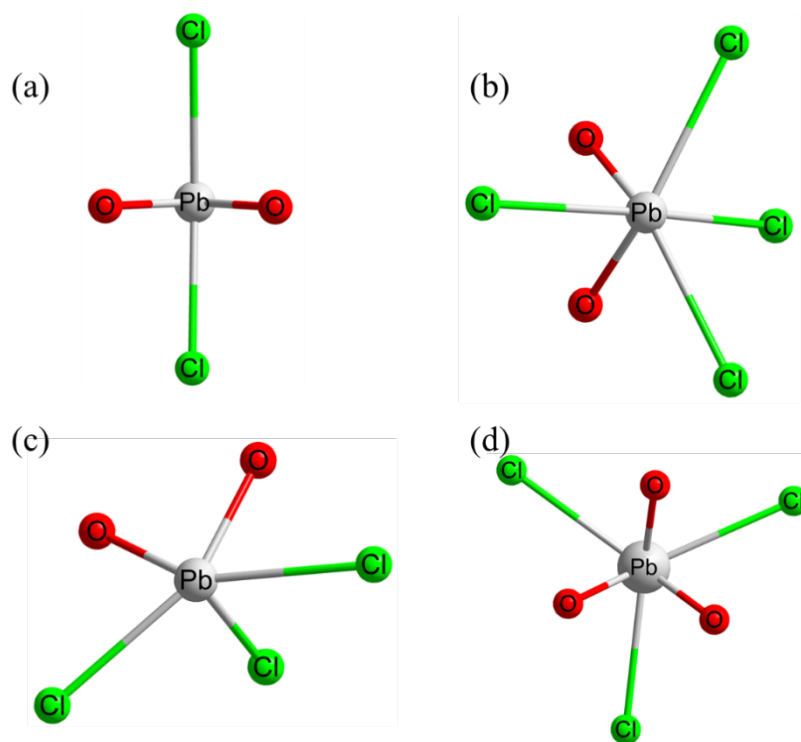
Figure S2. The structure of $[PbO_2Cl_4]$ (a) and $[PbO_2Cl_2]$ (b) in $Pb_3O_2Cl_2$;[17] (c) The structure of $[PbO_2Cl_3]$ in $Pb_{17}O_8Cl_{18}$;[18] (d) The structure of $[PbO3Cl3]$ in $Ba_{27}Pb_8O_8Cl_{54}$.[19]
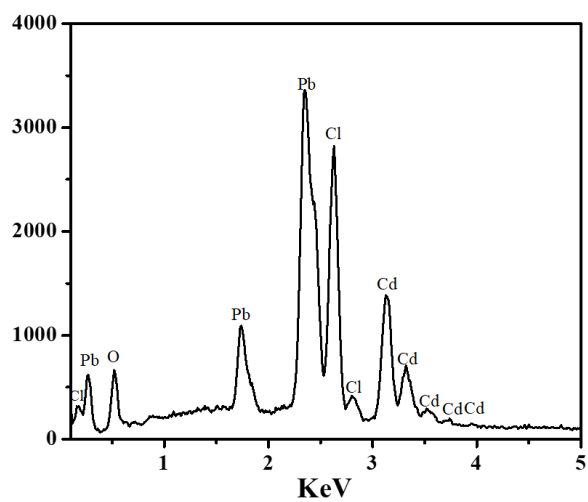
Figure S3. EDS spectrum of CdPbOCl$_2$ single crystal.
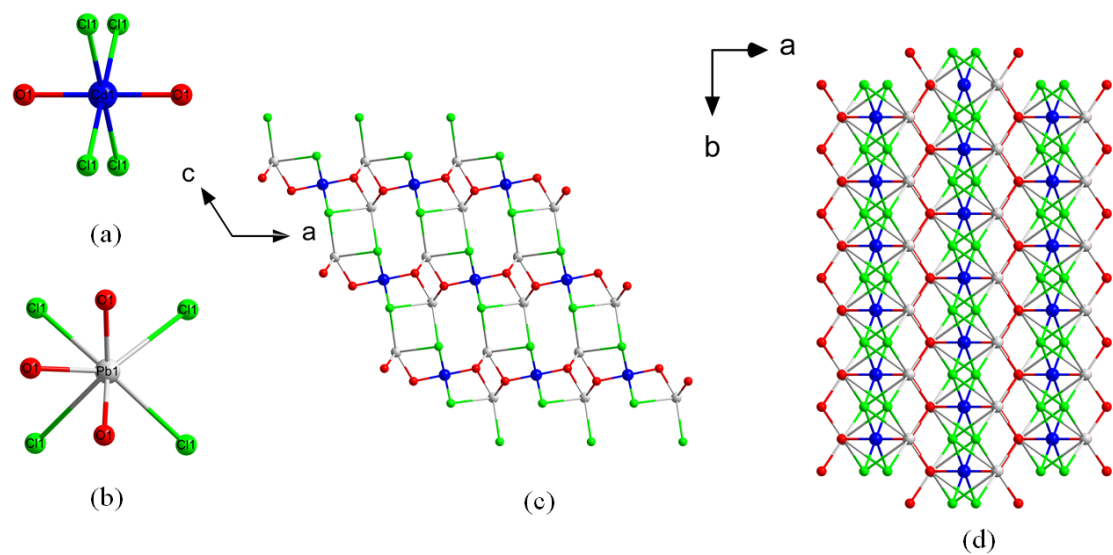
Figure S4. Crystal structure of $CdPb_2O_2Cl_2$. (a-b) The coordination of Cd and Pb atoms; (c-d) The Structure of $CdPb_2O_2Cl_2$ viewed along the b-axis and c-axis.
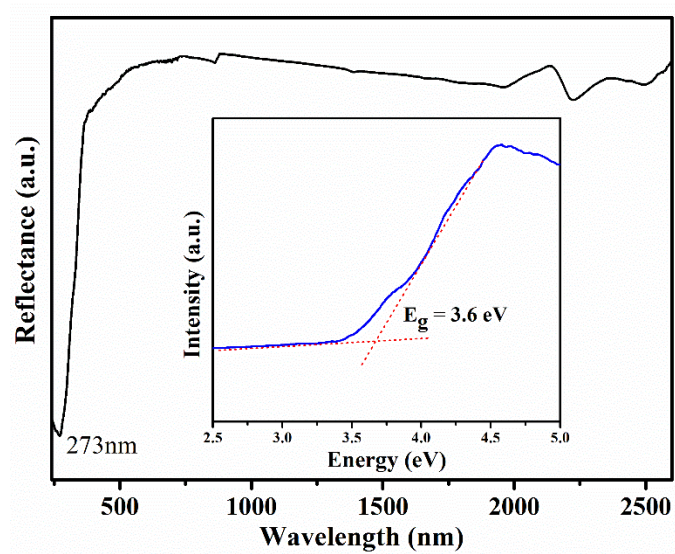
Figure S5. UV-vis-NIR diffuse spectrum and experiment band gap of $CdPbOCl_2$.
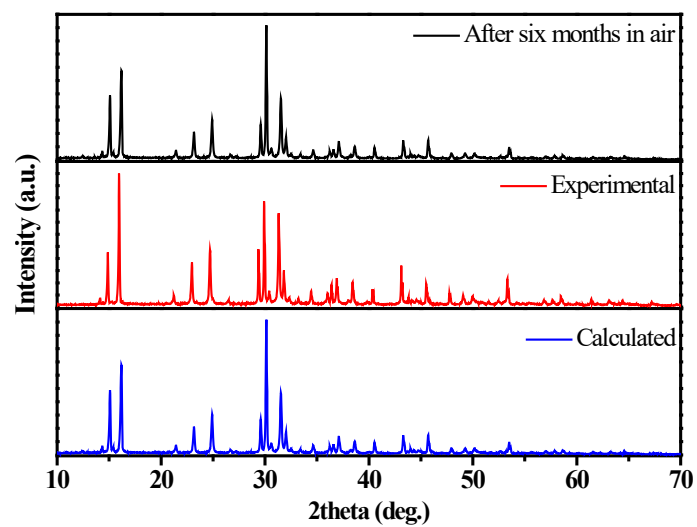
Figure S6. XRD patterns of polycrystalline CdPbOCl$_2$ samples before and after air-exposure for six months.
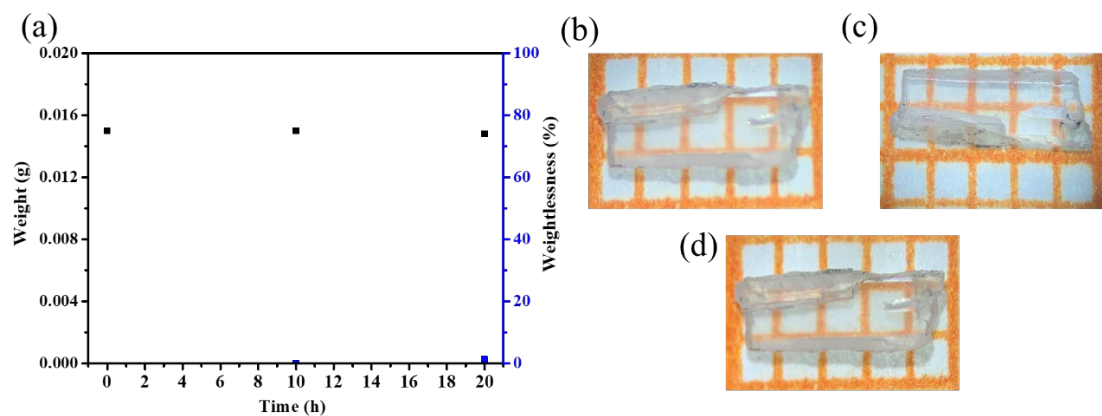
Figure S7. (a) Weight loss of CdPbOCl$_2$ single crystals before and after 50% humidity exposure for 10 h and 20 h; (b-d) Optical images of CdPbOCl$_2$ single crystals before and after 50% humidity exposure for 10 h and and 20 h.
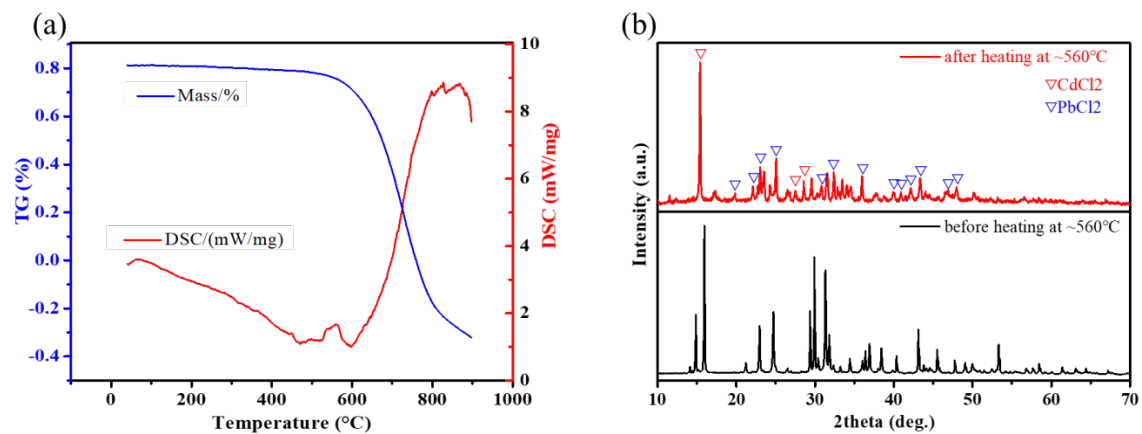
Figure S8. (a) TG-DSC curves of CdPbOCl$_2$; (b) The powder XRD results before and after heating at ~560 °C.
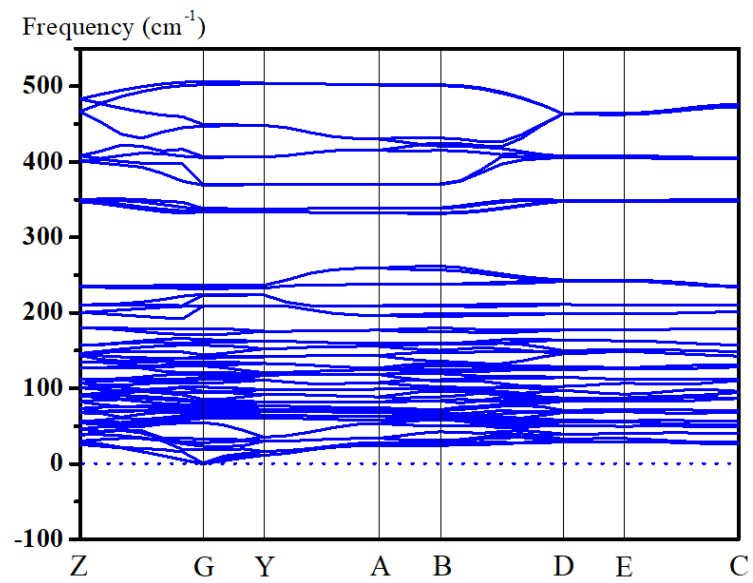
Figure S9. Calculated phonon spectrum of CdPbOCl$_2$.

References

1. G. M. Sheldrick, *Acta Crystallogr. C.*, 2015, **71**, 3.
2. H. W. Yu, H. P. Wu, S. L. Pan, Z. H. Yang, X. L. Hou, S. Xin, Q. Jing, K. R. Poeppelmeier and J. M. Rondinelli, *J. Am. Chem. Soc*. 2014, **136**, 1264.
3. H. P. Wu, H. W. Yu, S. L. Pan, Z. J. Huang and K. R. Poeppelmeier, *Angew. Chem. Int. Ed.*, 2013, **125**, 3490.
4. Y. Huang, K. Wu, J. N. Cheng, Y. Chu, Z. H. Yang and S. L. Pan, *Dalton Trans.*, 2019, **48**, 4484.
5. A. Abudurusuli, J. B. Huang, P. Wang, Z. H. Yang, S. L. Pan and J. J. Li, *Angew. Chem. Int. Ed.*, 2021.
6. J. Tauc, Mater. Res. Bull., 1970, **5**, 721.
7. J. Chen, C. L. Hu and J. G. Mao, Sci. China Mater., 2021, **64**, 400.
8. X.-M. Jiang, M.-J. Zhang, H.-Y. Zeng, G.-C. Guo and J.-S. Huang, *J. Am. Chem. Soc*. 2011, **133**, 3410.
9. L. J. Sham and M. Schlüter, Phys. Rev. Lett., 1983, **51**, 1888.
10. S. J. Clark, M. Segallii, C. J. Pickardii, P. J. Hasnipiii and M. Probertiv, *Z. Krist-Cryst. Mater.*, 2005, 220.
11. J. P. Perdew, K. Burke and M. Ernzerhof, *Phys. Rev. Lett.*, 1996, **77**, 3865.
12. A. M. Rappe, K. M. Rabe, E. Kaxiras and J. D. Joannopoulos, *Phys. Rev. B*, 1990, **41**, 1227.
13. A. V. Anyushin, D. A. Mainichev, N. K. Moroz, P. A. Abramov, D. Y. Naumov, M. N. Sokolov and V. P. Fedin, *Inorg. Chem.*, 2012, **51**, 9995.
14. J. L. Hoard and J. D. Grenko, *Z. Krist-Cryst. Mater.*, 1934, 87.
15. B.-P. Yang and J.-G. Mao, *J. Solid State Chem.*, 2014, **219**, 185.
16. Y. X. Song, M. Luo, F. Liang, C. Lin, N. Ye, G. Yan and Z. S. Lin, *Dalton Trans.*, 2017, 10.1039.C1037DT02573D.
17. O. I. Siidra, S. V. Krivovichev, T. Armbruster and W. Depmeier, *Z. Kristallogr.*, 2008, **223**, 204.
18. H. Zhang, M. Zhang, S. L. Pan, X. Y. Dong, Z. H. Yang, X. L. Hou, Z. Wang, K. B. Chang and K. R. Poeppelmeier, *J. Am. Chem. Soc.*, 2015, **137**, 8360.
19. D. Kucukcelebi and D. U. Sakarya, in Current Developments in Lens Design and Optical Engineering Xxi, eds. R. B. Johnson, V. N. Mahajan, S. Thibault, R. M. Bunch and C. C. Sun, 2020, vol. 11482.